Supplementary Online Material

Perfect conical nanoshape meets large magnetocrystalline anisotropy: unusual magnetic configuration

Jianzhuang Jiang,[a,b#] Wentao Wang,[b#] Xiaochan Fu,[a,b] Xinyan Wang,[a,b] Yuhui Hu,[a,b] Kaizhou He,[c] Xiangqian Wang*[c] and Xia Ni*[a]

[a.] *School of Materials and Energy, Lanzhou University, Lanzhou 730000, China*

[b.] *Institute of Modern Physics, Chinese Academy of Sciences, Lanzhou 730000, China*

[c.] *Key Laboratory of Sensor and Sensor Technology, Institute of Sensor Technology, Gansu Academy of Sciences, Lanzhou 730000, China*

Figure S1. Sample fabrication. In this work, we adopted the ion-track template method and electrochemical deposition to prepare Co nanocone arrays. The main fabrication processes employed are schematically demonstrated in Fig. S1. Polycarbonate (PC) foils of 12 μm in thickness were first irradiated with normal beam incidence of ^{129}Xe ions (total energy of 771 MeV, step 1) accelerated by the Heavy Ion Research Facility in Lanzhou (HIRFL). The irradiation fluence was 2.5×10^7 cm^{-2}. This step is followed by the sputtering of an Au film (~30 nm in thickness) onto one surface of the PC foils which serves as the cathode for the subsequent asymmetric etching of ion tracks (step 2). To facilitate the removal of the Au film and to increase the support of the foils, a 15 μm thick Cu layer was electrodeposited on the gold surface (step 3). The Cu electrolyte was composed of 0.3 M $CuSO_4 \cdot 5H_2O$ + 0.3 M H_2SO_4. Subsequently, the ion tracks are etched by asymmetric etching to produce conical channels (step 4). The shape of etched channels is totally determined by the competition between the etch rates of NaOH and methanol. The maximum length of nanocones is governed by

the template thickness and may be changed by controlling the electrodeposition time. When a steady voltage of 0.2 V is provided, the electrical current flowing across the foils is measured to monitor the etching process. Co nanocones are synthesized in the channels using electrochemical deposition (step 5). Co nanocones were electrochemically deposited using a direct current voltage of 1.35 V at 50 ℃. The composition of the electrolyte was 0.9 M $CoSO_4 \cdot 7H_2O$ + 0.2 M $CoCl_2 \cdot 6H_2O$ + 0.5 M H_3BO_3. The pH of electrolyte was adjusted by adding 1 M sodium hydroxide solution or diluting hydrochloric acid solution. Finally, because of the weak binding force between the Au/Cu layer and the foils, the Au/Cu layer may be easily peeled off, leaving nanocone arrays implanted in the foils (step 5).

For control experiments, Co nanowire arrays were synthesized by using the same method but within cylindrical channels. To this end, each side of the irradiated PC foils was exposed to ultraviolet light for 2 hours to enhance the track etching rate. Next,

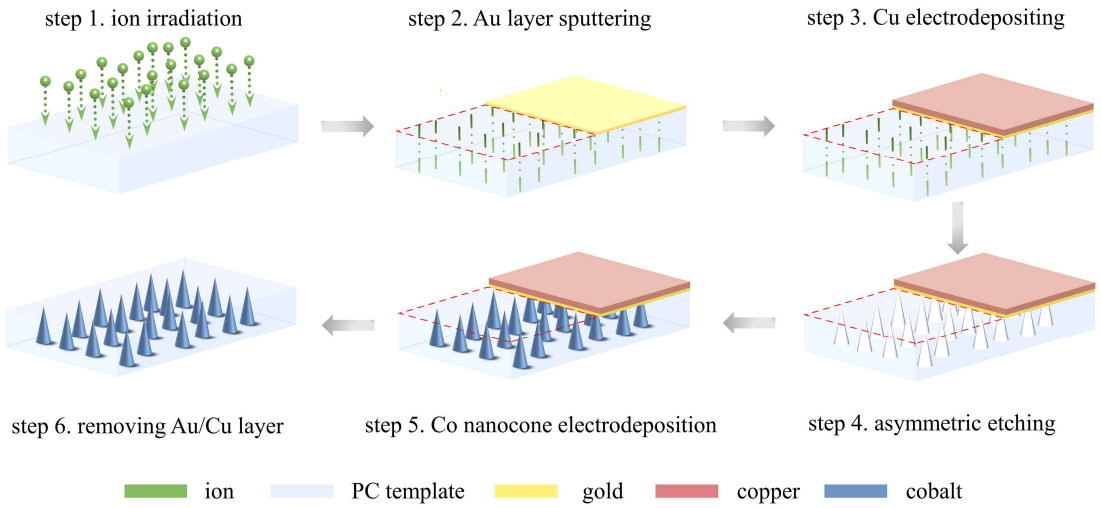

Fig. S1. Schematic fabrication procedures of Co nanocone arrays based on ion-track template and electrochemical deposition. Ion irradiation of PC foils (step 1), sputtering of gold film (step 2), electrochemical deposition of copper layer (step 3), asymmetric etching of ion tracks to form conical channels (step 4), electrochemical deposition of Co nanocones in conical channels (step 5), and detaching Au/Cu layer by peeling-off (step 6).

the foils were chemically etched in a 9 M NaOH solution at 50 ℃. To obtain cylindrical channels with diameters of 100 nm and 500 nm, the chemical etching time was set to 2.5 minutes and 12 minutes, respectively. Co nanowires were electrochemically deposited in the electrolyte at pH=3.0.

Figure S2. Morphological characterizations of the as-fabricated Co nanowires. To investigate the difference in magnetic configuration between nanocones and cylindrical nanowires, we prepared nanowires of 100 nm and 500 nm between the diameter of the tip and the bottom of the cone. In Fig. S2, the SEM image shows that the nanowire surface is also smooth. The length of the nanowires is about 10 μm. Note that NW1 is aggregated at tip region. Such surface-tension-induced aggregation happened during the dissolving of the PC template.

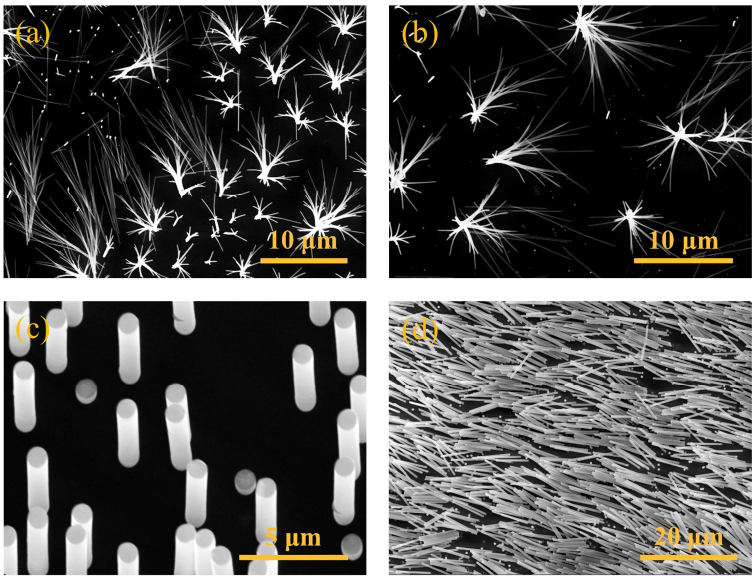

Fig. S2. Morphological characterizations of the as-fabricated Co nanowires. (a-b) SEM micrographs of NW1, (c-d) SEM micrographs of NW2.

Figure S3. FORC diagrams of NC1. To better understand the angular dependence of the magnetic properties of NC1, we measured FORCs at different angles of *H* with respect to the cone axis direction, from θ= 0° to 90°, in 15° steps (Fig. S3). The T-shape

is retained from θ = 0° to 45°, but the interaction field increases. The coercivity presents a maximum at 60° when a reversible event occurs and the coercivity presents a maximum.

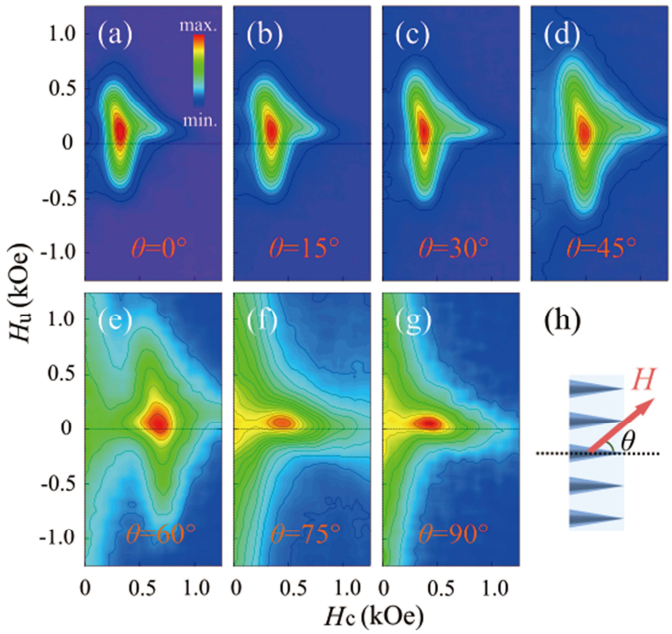

Fig. S3. FORC diagrams of NC1 nanocone arrays for (a) θ = 0°, (b) θ = 15°, (c) θ = 30°, (d) θ = 45°, (e) θ = 60°, (f) θ = 75°, and (g) θ = 90°. (h) Schematic representation of the angle between the applied field and cone length (θ).

Figure S4. A quantitative analysis of the FORC diagram of the NC1 sample. In this section, we performed a quantitative analysis of the FORC measurement of the NC1 sample. Fig. S4a shows the cross-section of the FORC diagrams along the H_c axis for the NC1. To estimate ΔH_u we fitted the peak profile of the FORC diagram observed along the H_u axis using a Gaussian function and extracted the values of the full width at half-maximum. The half-width of the FORC distribution along the H_u axis (ΔH_u) can be used as an estimative value of the interaction field between the nanocones at saturation. Fig. S4b shows the cross-section of the FORC diagram along the H_u axis for the NC1 at θ = 0° and θ = 45°. We can see that ΔH_u=654 Oe at 0° is smaller than

ΔH_u=924 Oe at 45°. The main reason is that the exchange interaction caused by the conical shape creates more magnetic moments distributed in-plane. The quantitative results of the different magnetometry as a function θ have also been compared and summarized in Fig. S4c. All three are increasing and then decreasing, and there is a transition angle, because FORC measures the local magnetization reversal, thus leading to a slight difference in the position of the transition angle.

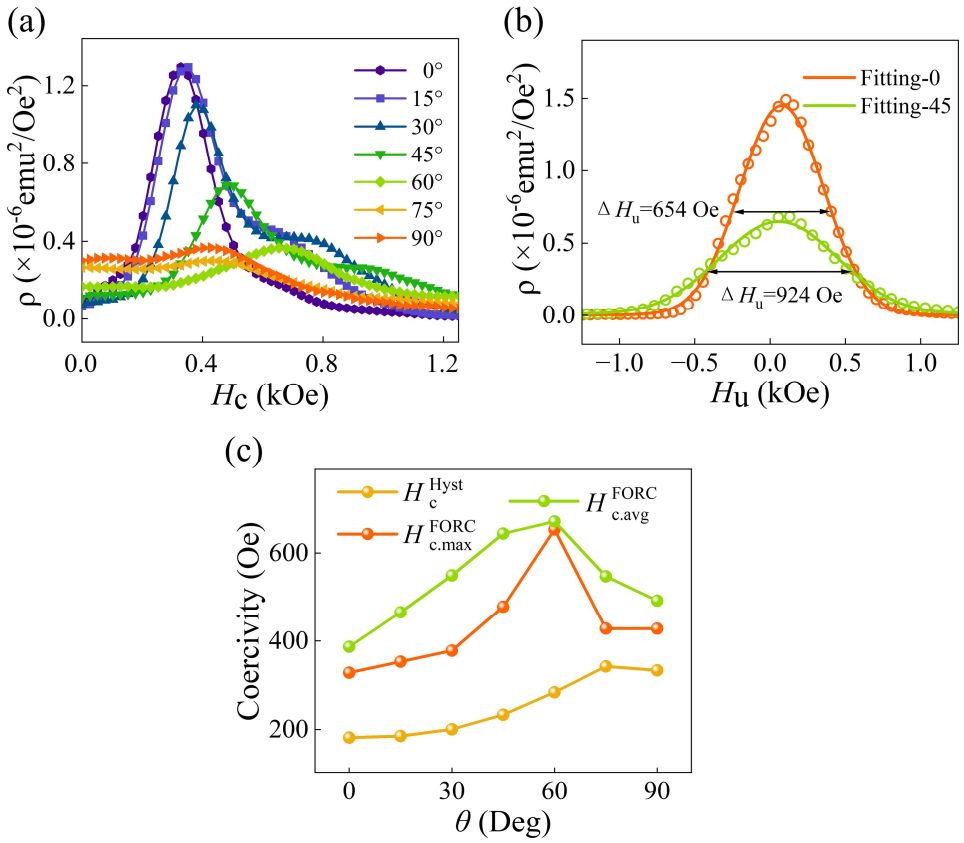

Fig. S4. A quantitative analysis of the FORC diagram of the NC1sample. (a) Cross sectional view of FORC diagram along the H_c axis crossing from maximum contribution when θ is between 0° and 90° in 15° steps, (b) cross sectional view of FORC diagram along the H_u axis crossing from maximum contribution with θ = 0° and θ = 45°, (c) comparison of the coercivity.

Figure S5. FORC diagrams of NC2. In this section, we know the FORC diagram is a superposition of two separate FORC distributions. As the angle increases, the coercivity also increases correspondingly, reaching a peak at θ = 60°. The interaction

field along the H_u axis direction also gradually expands. At θ = 75°, the FORC diagrams display increasing reversible reversal events and finally change to multidomain.

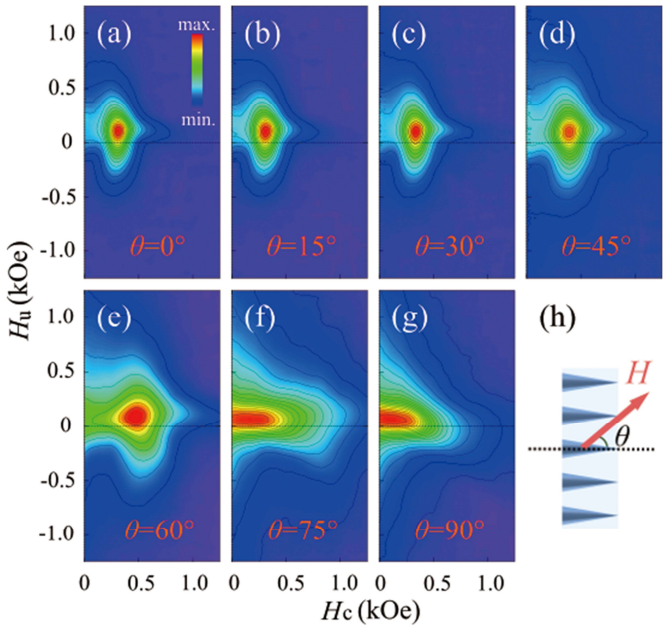

Fig. S5. FORC diagrams of NC2 for (a) θ = 0°, (b) θ = 15°, (c) θ = 30°, (d) θ = 45°, (e) θ = 60°, (f) θ = 75°, and (g) θ = 90°. (h) Schematic representation of the angle between the applied field and cone length (θ).

Figure S6. FORC diagrams of NC3. The NC3 displays a multidomain feature from 0° to 90°. At θ = 60°, the spread distributed along the -H_u axis direction at high coercivity disappears and a large tail along the H_c axis direction emerges, probably due to the strong in-plane energy.

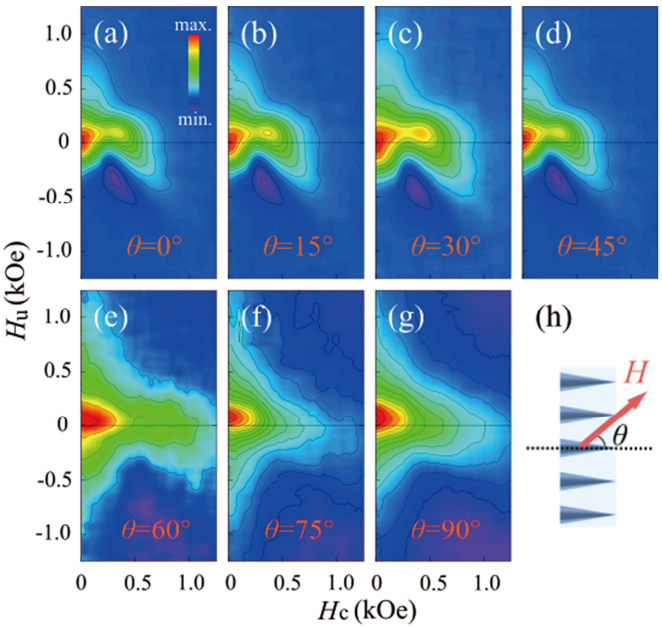

Fig. S6. FORC diagrams of NC3 for (a) θ = 0°, (b) θ = 15°, (c) θ = 30°, (d) θ = 45°, (e) θ = 60°, (f) θ = 75°, and (g) θ = 90°. (h) Schematic representation of the angle between the applied field and cone length (θ).

Figure S7. The FORC diagrams for Co nanowires. To further analyze the magnetic configuration between Co nanocones and nanowires, the FORC method has also been performed. The resulting FORC diagrams for NC4, NW1, and NW2 at θ = 0° and θ = 90° are presented in Fig. S7. As previously noted, θ = 0° is the direction along the longitudinal axis, which is parallel to the demagnetization field and perpendicular to the magnetocrystalline anisotropy field. The NW1 exhibits quasi-single-domain behavior with low interaction fields about 200 Oe at θ = 0°, while the NC4 and NW2 behave in multidomain configurations. For θ =90°, the external magnetic field was applied perpendicular to the nanostructure longitudinal axis. The FORC diagrams share some common features such as reversible events and an elongated distribution along the H_u axis. The FORC diagrams share some common features, such as reversible events and an elongated distribution along the H_u axis, which is the case as a result of

the in-plane magnetization leading to the magnetostatic interaction between packed cones. The exchange interaction and magnetocrystalline anisotropy create more magnetic moments distributed in-plane. The exchange interaction caused by the conical shape and the anisotropy of the magnetocrystalline anisotropy with specific orientation create more magnetic moment distributed in-plane.

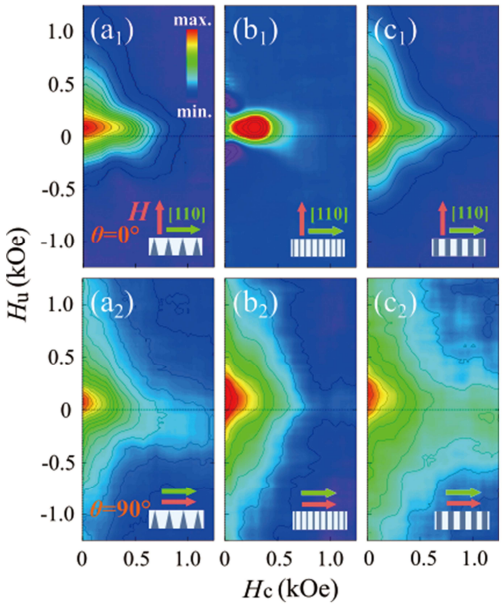

Fig. S7. FORC diagrams of the NC4 (a_1-a_2), NW1 (b_1-b_2), and NW2 (c_1-c_2) at θ = 0° and θ = 90°.